Pushing the Limits in Real-Time Measurements of Quantum Dynamics

E. Kleinherbers[,1,*] P. Stegmann[,2,†] A. Kurzmann[,3] M. Geller[,1] A. Lorke[,1] and J. König[1]

[1]*Faculty of Physics and CENIDE, University of Duisburg-Essen, 47057 Duisburg, Germany*
[2]*Department of Chemistry, Massachusetts Institute of Technology, Cambridge, Massachusetts 02139, USA*
[3]*2nd Institute of Physics, RWTH Aachen University, 52074 Aachen, Germany*

Time-resolved studies of quantum systems are the key to understanding quantum dynamics at its core. The real-time measurement of individual quantum numbers as they switch between certain discrete values, well known as a "random telegraph signal," is expected to yield maximal physical insight. However, the signal suffers from both systematic errors, such as a limited time resolution and noise from the measurement apparatus, as well as statistical errors due to a limited amount of data. Here we demonstrate that an evaluation scheme based on factorial cumulants can reduce the influence of such errors by orders of magnitude. The error resilience is supported by a general theory for the detection errors as well as experimental data of single-electron tunneling through a self-assembled quantum dot. Thus, factorial cumulants push the limits in the analysis of random telegraph data, which represent a wide class of experiments in physics, chemistry, engineering, and life sciences.

Resolving dynamics of open quantum systems [1] on the most fundamental level of individual quantum events is a common goal in many fields of science. Real-time measurements have been performed for a large variety of quantum systems, including ions [2], neutral atoms [3,4], single molecules [5–10], and skyrmions [11]. Fluctuating occupation numbers of optical and plasmonic cavities [12,13], metallic islands [14], quantum dots [15–19], trapped quantum gases [20], and nanocalorimeters [21,22] have been measured with single-photon, -electron, -atom, and -ion precision.

These experiments record in time switches between distinct quantum states, as illustrated by the black line in Fig. 1. The form of the depicted time evolution is known as a random telegraph signal. It can provide information about hidden quantum states, such as degenerate spin states [19] or dark states [13]. Underlying interactions such as magnetic [3,4] or attractive electron-electron interactions [23] as well as internal quantum transitions such as spin relaxation [24] or conformational changes in single molecules [5–10] and even non-equilibrium phase transitions [25,26] can be revealed. Unfortunately, the measured signal (green line) suffers from problems that appear in any detection scheme: fast transitions are overlooked (indicated by *A* and *C*) due to a limited time resolution, false transitions (indicated by *B* and *D*) are recorded due to a noisy detector signal, and statistical errors occur due to the finite time span over which data are collected.

There are many experimental attempts to overcome these problems, e.g., by employing high-bandwidth detection [24], noise-suppression techniques [27–30], or quantum stochastic resonance [31]. As a complementary strategy to push the limits set by typical detection errors, we suggest employing a specific statistical tool set, i.e., "factorial cumulants," for the analysis of random telegraph data. Factorial cumulants are well known from a mathematical perspective [32] and designed to characterize discrete probability distributions [33], in contrast to ordinary cumulants, which are designed for continuous probability distributions. Therefore, it is much more natural to use factorial cumulants for the analysis of random telegraph data, where transitions between discrete states are investigated. Moreover, factorial cumulants are expected to be sensitive indicators for correlation [23,34–37]. Nonetheless, their full potential has so far only been little explored for practical evaluation of (noisy) statistical data. This is very unfortunate since, as we show in this Letter, factorial cumulants are resilient to errors that otherwise obscure the quantum dynamics of interest and may result in a wrong modeling of the quantum system.
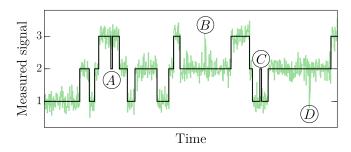

FIG. 1. Generic form of a random telegraph signal (green) that deviates from the true quantum dynamics (black) because of events that are missed (*A* and *C*) or falsely indicated (*B* and *D*) by the detector. Simulated data are depicted.
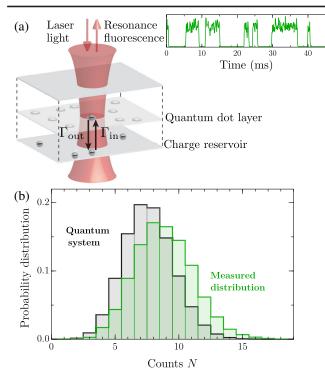
FIG. 2. (a) Experimental setup for the optical readout of the electron occupation of a self-assembled quantum dot. The measured resonance-fluorescence signal is depicted in green. (b) Measured probability distribution P_N^{meas} (green) compared with the distribution P_N (black) that originates from the true quantum dynamics for a time interval $t = 45$ ms.

To illustrate this concept, we study temporal charge fluctuations of a self-assembled semiconductor quantum dot with single-electron precision. The setup is depicted in Fig. 2(a). The quantum dot is tunnel coupled to an external charge reservoir, so that single electrons can tunnel into and out of the quantum dot with rates Γ_{in} and Γ_{out}, respectively. Because of a strong Coulomb repulsion, the quantum dot is either empty or occupied by one electron only. The occupation of the quantum dot is monitored using a resonance-fluorescence readout scheme [24,38–40]. If the quantum dot is empty, an infrared laser drives an excitonic transition and the emitted fluorescence photons are collected by a single-photon detector. If the quantum dot is occupied, no photons are emitted. After binning the measured stream of single photons with an adjustable binning time, the bright state (empty quantum dot) and the dark state (occupied quantum dot) can be resolved as a function of time; see the resonance-fluorescence signal in Fig. 2(a) depicted in green. The setup yields a high-quality telegraph signal with almost negligible errors as a reference measurement. Nevertheless, we can artificially increase the detection errors by either modifying the time resolution or removing a large fraction of the collected photons and thus "blinding" the detector.

The measured telegraph signal contains much more information than just the mean number $\langle N \rangle$ of tunneling

events. In particular, the fluctuations around this mean value have a strong predictive power about the properties of the quantum system [41]. In the framework of full counting statistics, the information of these fluctuations is summarized in the probability distribution $P_N^{\mathrm{meas}}(t)$ that N tunneling events have been counted in a time interval of length t [green histogram in Fig. 2(b)], where we use the convention to count only tunneling-out events.

The measured probability distribution P_N^{meas} can be systematically analyzed by its ordinary cumulants κ_m of order m [42]. The first cumulant $\kappa_1 = \langle N \rangle$ describes the mean and the second cumulant $\kappa_2 = \langle N^2 \rangle - \langle N \rangle^2$ the variance of the distribution. With increasing order m, successively more details about P_N^{meas} are revealed. The cumulants can be derived from the generating function

$$S^{\mathrm{meas}}(z) = \ln\left(\sum_N z^N P_N^{\mathrm{meas}}\right), \qquad (1)$$

via $\kappa_m = \partial_\chi^m S^{\mathrm{meas}}(e^\chi)\big|_{\chi=0}$ [42], where we introduce the counting variable z. In Fig. 3(a), the ordinary cumulants κ_m (dots) are depicted as a function of time t. As the order m increases, the time dependence $\kappa_m(t)$ acquires more and more structure. However, this is merely part of a general property of ordinary cumulants, referred to as universal oscillations [17], and hence contains no system-specific information. Therefore, it has been suggested to use factorial cumulants $C_{F,m}(t)$ instead [35], which are defined by $C_{F,m} = \partial_z^m S^{\mathrm{meas}}(z)\big|_{z=1}$. They are related to ordinary cumulants by $C_{F,m} = \sum_{j=1}^m s_{m,j}\kappa_j$, with the Stirling numbers of the first kind $s_{m,j}$ giving the coefficients of the factorial power [32]. In fact, in Fig. 3(b), the factorial cumulants $C_{F,m}$ (dots) do not show such universal oscillations and, thus, are much better suited to extract physical information.

In this Letter, we demonstrate an even more remarkable advantage of factorial cumulants, namely, their robustness against errors, which is also clearly visible in Figs. 3(a) and 3(b). We compare the measured cumulants (dots) with the theoretical limit (solid lines) of an ideal measurement with infinite bandwidth and signal-to-noise ratio, as well as an unlimited amount of data. While the ordinary cumulants $\kappa_m(t)$ in Fig. 3(a) are heavily influenced by the measurement imperfections, the factorial cumulants $C_{F,m}(t)$ in Fig. 3(b), on the other hand, are error resilient. The relative error depicted in Fig. 3(c) increases drastically for the ordinary cumulants $\kappa_m(t)$ with each order m and surpasses 100% beginning with the fourth ordinary cumulant at finite times. In contrast, the error of the factorial cumulants $C_{F,m}(t)$ at finite times remains at around 1% for all orders $m > 1$.

To explain the ruggedness of factorial cumulants against measurement imperfections, we need to faithfully model the measured probability distribution P_N^{meas}. In any
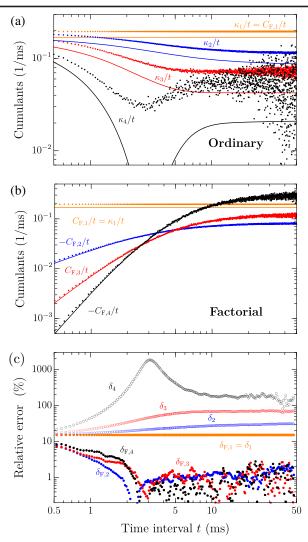
FIG. 3. (a) Ordinary cumulants κ_m/t, (b) factorial cumulants $C_{F,m}/t$, and (c) their relative errors δ_m and $\delta_{F,m}$ as a function of time t. Experimental data (dots) are compared with a simulation disregarding measurement imperfections (solid lines). Relative errors in (c) are obtained by averaging over 20 successive data points to reduce statistical errors. The time resolution is $\Delta t = 50$ μs, the false-count rate of the bright state is $\Gamma_0^{\text{false}} = 0.059$ kHz, and the duration of the measurement is $T = 369$ s. The electron-tunneling rates are $\Gamma_{\text{in}} = 0.346$ kHz and $\Gamma_{\text{out}} = 0.334$ kHz.

detection scheme, the probability distribution is inevitably subjected to errors and, thus, can be decomposed as

$$P_N^{\text{meas}} = \sum_{N'=0}^{N} P_{N-N'}\delta P_{N'}^{\text{sys}} + \delta P_N^{\text{sta}}. \quad (2)$$

The desired information about the electron-tunneling events is contained in P_N [black histogram in Fig. 2(b)]. In contrast, δP_N^{sys} accounts for the systematic error due to missed and false events, and δP_N^{sta} represents the statistical

error caused by the finite measurement time. Accordingly, we can write the generating function from Eq. (1) as

$$S^{\text{meas}} = S + \delta S^{\text{sys}} + \delta S^{\text{sta}}. \quad (3)$$

The function $S = \ln(\sum z^N P_N)$ is related via $P_N = \text{tr}[\rho_N(t)]$ to the quantum system's density matrix ρ_N with the constraint that N tunneling-out events have occurred in the time interval $[0, t]$. The time evolution of ρ_N is governed by the N-resolved master equation [43,44]

$$\dot{\rho}_N = (\mathcal{W} - \mathcal{J}_{\text{out}})\rho_N + \mathcal{J}_{\text{out}}\rho_{N-1}, \quad (4)$$

where $\mathcal{W}$ is the generator of the full time evolution, while $\mathcal{J}_{\text{out}} = \mathcal{P}_0\mathcal{W}\mathcal{P}_1$ describes the tunneling-out events from the occupied (projector $\mathcal{P}_1$) to the empty (projector $\mathcal{P}_0$) quantum dot. The solution of the master equation is readily obtained after a z transform and reads $\rho_z = \sum_N z^N \rho_N = e^{\mathcal{W}_z t}\rho_{\text{st}}$ with the generator $\mathcal{W}_z = (\mathcal{W} - \mathcal{J}_{\text{out}}) + z\mathcal{J}_{\text{out}}$. The stationary state of the quantum system ρ_{st} has been reached before the counting starts. Finally, tracing out the quantum degrees of freedom leads to the generating function [1,44]

$$S = \ln \text{tr}(e^{\mathcal{W}_z t}\rho_{\text{st}}). \quad (5)$$

A unified theoretical description of the errors δS^{sys} and δS^{sta} has been missing in the literature so far. However, neglecting them may result in a huge discrepancy between experiment and (error-free) theoretical model, as illustrated in Fig. 3(a). To close this gap, we developed a general model that accounts for measurement imperfections and can be applied to an arbitrary quantum system and an arbitrary set of detected and undetected quantum transitions, see Sec. I of the Supplemental Material [45]. Using the quantum dot system as an example, we present here the steps to incorporate the errors into the theoretical model which is illustrated in Fig. 4.

First, we take into account that the quantum dot state is measured with a limited time resolution Δt. Therefore, the counter N is not introduced on the level of the master equation (4), but on the level of the coarse-grained time evolution

$$\rho_N(t + \Delta t) = (\Pi - \mathcal{P}_0\Pi\mathcal{P}_1)\rho_N(t) + \mathcal{P}_0\Pi\mathcal{P}_1\rho_{N-1}(t), \quad (6)$$

which ensures that at each time step Δt the counter N increases at most by one. Here, $\Pi = e^{\mathcal{W}\Delta t}$ propagates the quantum state in steps of Δt. Transitions from the empty (0) to the occupied dot (1) and vice versa happen at each time step Δt with probability p_{in} and p_{out}, respectively. With probability $1 - p_{\text{in}}$ and $1 - p_{\text{out}}$, the state does not change.

Second, to account for a faulty detector, whose output may deviate from the actual quantum state, we explicitly introduce the detector degree of freedom. Therefore, we resolve the density matrix according to $\boldsymbol{\varrho}_N = (\rho_N^{(0)}, \rho_N^{(1)})$,
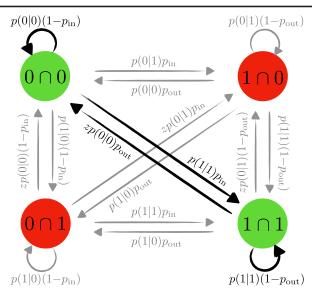
FIG. 4. Four-dimensional model to simulate both a limited time resolution and noise. The possible states are indicated via $a \cap b$ denoting that the measurement outcome is b and the true value is a. True associations $b = a$ are colored in green and false associations $b \neq a$ are colored in red. At each time step Δt, the states are updated due to true tunneling events with transition probabilities p_{in} and p_{out} and false noise-induced events with probabilities $p(b|a)$. Noise-related transitions are indicated as gray arrows. Transitions increasing the detector counter N are multiplied by z.

where the superscript (b) with $b \in \{0, 1\}$ denotes the state indicated by the detector. Thus, the density matrix element $\langle a| \rho^{(b)} |a\rangle = p(a \cap b)$ gives the joint probability that the detector output is b and the quantum dot state is $|a\rangle$ with $a \in \{0, 1\}$. In Fig. 4, true associations $a = b$ are shown in green and false associations $a \neq b$ are shown in red. The N-resolved time evolution becomes

$$\boldsymbol{\varrho}_N(t + \Delta t) = (\boldsymbol{\Pi} - \mathcal{P}^{(0)} \boldsymbol{\Pi} \mathcal{P}^{(1)}) \boldsymbol{\varrho}_N(t) + \mathcal{P}^{(0)} \boldsymbol{\Pi} \mathcal{P}^{(1)} \boldsymbol{\varrho}_{N-1}(t), \tag{7}$$

where the projectors $\mathcal{P}^{(b)}$ for the detector states ensure that the counter N is only sensitive to changes of the detector output. The propagator is given by $\boldsymbol{\Pi} = \mathcal{F} \cdot (\mathcal{D} \otimes e^{\mathcal{W} \Delta t})$ with $(\mathcal{D})_{bb'} = 1$. Here, the diagonal matrix $\mathcal{F} = \text{diag}[p(0|0), p(0|1), p(1|0), p(1|1)]$ accounts for false detector outputs, where $p(b|a)$ are the conditional probabilities that we measure b, given that the true value is a. They fulfill $\sum_b p(b|a) = 1$. Thus, at each time step Δt, the detector indicates with a probability $p(0|1)$ an empty and with $p(1|0)$ an occupied quantum dot, although the actual state is the opposite, see Fig. 4. False transitions of the form $0 \rightarrow 1$ and $1 \rightarrow 0$ (similar to B and D in Fig. 1) are the consequence. The type of the noise and Δt determine the specific values of the conditional probabilities $p(b|a)$.

To solve Eq. (7), we perform a z transform and find

$$\boldsymbol{\varrho}_z(t + \Delta t) = \boldsymbol{\Pi}_z \boldsymbol{\varrho}_z(t) = \mathcal{F} \cdot (\mathcal{D}_z \otimes e^{\mathcal{W} \Delta t}) \boldsymbol{\varrho}_z(t), \tag{8}$$

with $(\mathcal{D}_z)_{bb'} = 1 + (z - 1)\delta_{b0}\delta_{1b'}$. Starting from the stationary state $\boldsymbol{\varrho}_{\text{st}}$, we apply Eq. (8) successively to arrive at $\boldsymbol{\varrho}_z(t) = \boldsymbol{\Pi}_z^{t/\Delta t} \boldsymbol{\varrho}_{\text{st}}$. Finally, we trace out the quantum degrees of freedom and obtain the full generating function

$$S^{\text{meas}} = \ln \text{tr}(\boldsymbol{\Pi}_z^{t/\Delta t} \boldsymbol{\varrho}_{\text{st}}) + \delta S^{\text{sta}}. \tag{9}$$

The term δS^{sta} accounting for the statistical error can be derived via the central limit theorem, see Sec. I C of the Supplemental Material [45].

By employing our model, we are finally able to explain the experimental results. We illustrate the impact of the different error sources separately in Fig. 5(a) for the fourth ordinary cumulant κ_4. To obtain experimental data (black dots) with both a bad time resolution and many noise-induced false counts, we randomly deleted 95% of all
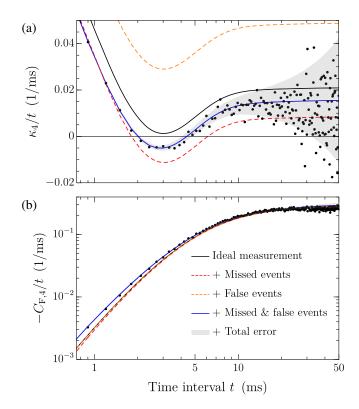

FIG. 5. (a) Fourth ordinary cumulant κ_4/t and (b) fourth factorial cumulant $-C_{F,4}/t$ as a function of time t. Experimental data (black dots) are compared with theoretical calculations, including no error (black line), only a limited time resolution (red dashed line), only noise (orange dashed line), and both together (blue solid line). In gray, we indicate the statistical error due to a finite measurement time. The time resolution is $\Delta t = 300\ \mu$s, the false-count rate of the bright state is $\Gamma_0^{\text{false}} = 0.038$ kHz, and the duration of the measurement is $T = 369$ s. The electron-tunneling rates are $\Gamma_{\text{in}} = 0.346$ kHz and $\Gamma_{\text{out}} = 0.334$ kHz.

detected photons. The theoretical results (lines) are derived from Eq. (9). If we do not consider any error in our model (black solid line), the theory clearly deviates from the experiment (black dots). If we include only the noise-induced error (orange dashed line), then we overshoot, and if we include only the error due to the limited time resolution (red dashed line), then we undershoot. Only by considering both errors simultaneously (blue solid line), we find a nice agreement between theory and experiment. The continuous error bars that we obtained from δS^{sta} [shaded area in Fig. 5(a)] capture the statistical fluctuations around the blue curve due to the limited amount of data. In contrast, for the fourth factorial cumulant $C_{F,4}$ illustrated in Fig. 5(b), both the false and missed events have almost no effect, even though we used a poor time resolution $\Delta t = 300\ \mu$s and randomly deleted 95% of all detected photons. In addition, a limited amount of data leads to only relatively weak statistical fluctuations, see Sec. III B of the Supplemental Material [45].

To elucidate why factorial cumulants $C_{F,m}$ possess a built-in ruggedness against measurement imperfections, we study the limit of small errors by performing a consistent perturbation expansion in the time resolution Δt and the false-count rates $\Gamma_0^{\mathrm{false}} := p(1|0)/\Delta t$ and $\Gamma_1^{\mathrm{false}} := p(0|1)/\Delta t$. Starting with the expression given in Eq. (8), which is valid for arbitrarily strong measurement imperfections, we find

$$\dot{\rho}_z = (\mathcal{W}_z + \mathcal{W}_z^{\mathrm{miss}} + \mathcal{W}_z^{\mathrm{false}})\rho_z, \qquad (10)$$

where, in addition, we performed a partial trace over the detector degrees of freedom, $\rho_z = \sum_b \rho_z^{(b)}$. Thus, the errors of missing $\mathcal{W}_z^{\mathrm{miss}}$ and false events $\mathcal{W}_z^{\mathrm{false}}$ enter as effective corrections to the actual quantum dynamics encoded in $\mathcal{W}_z$. In particular, we find $\mathcal{W}_z^{\mathrm{miss}} = -(z-1)\Delta t(\mathcal{J}_{\mathrm{in}}\mathcal{J}_{\mathrm{out}} + \mathcal{J}_{\mathrm{out}}\mathcal{J}_{\mathrm{in}})/2$, which describes successive tunneling-in ($\mathcal{J}_{\mathrm{in}} = \mathcal{P}_1\mathcal{W}\mathcal{P}_0$) and tunneling-out ($\mathcal{J}_{\mathrm{out}} = \mathcal{P}_0\mathcal{W}\mathcal{P}_1$) events too close to each other to be resolved by the detector (similar to A and C in Fig. 1). This leads to missing counts. The false events due to noise are described by the diagonal matrix $\mathcal{W}_z^{\mathrm{false}} = (z-1)\mathrm{diag}(\Gamma_0^{\mathrm{false}}, \Gamma_1^{\mathrm{false}})$. With rate $\Gamma_a^{\mathrm{false}}$, the telegraph signal suffers from spurious switches to neighboring values $b \neq a$ and back again to a (similar to B and D in Fig. 1). Accordingly, we find for the generating function

$$S^{\mathrm{meas}} = \ln\ \mathrm{tr}(e^{\mathcal{W}_z t + \mathcal{W}_z^{\mathrm{miss}}t + \mathcal{W}_z^{\mathrm{false}}t}\rho_{\mathrm{st}}) + \delta S^{\mathrm{sta}}, \qquad (11)$$

where the errors of missing ($\mathcal{W}_z^{\mathrm{miss}}$) and false ($\mathcal{W}_z^{\mathrm{false}}$) events still enter in a complicated way. However, the expression simplifies considerably in the limit of short time intervals t. Then, the systematic error reads

$$\delta S^{\mathrm{sys}} = (z-1)(\Gamma^{\mathrm{false}} - \Gamma^{\mathrm{miss}})t, \qquad (12)$$

with the mean rates $\Gamma^{\mathrm{false/miss}} = \pm\partial_z\mathrm{tr}(\mathcal{W}_z^{\mathrm{false/miss}}\rho_{\mathrm{st}})|_{z=0}$. As a result, the corrections due to false and missing events turn out to be Poisson-like with positive and negative prefactors, respectively. This is true even for arbitrary times t if both $\mathcal{W}_z^{\mathrm{false}} \propto \mathbb{1}$ and $\mathcal{W}_z^{\mathrm{miss}} \propto \mathbb{1}$, i.e., if the false and missed events happen independently of the quantum state. In our experimental setup, however, the bright-state intensity fluctuates much more than the dark-state signal [see Fig. 2(a)], and, therefore, the false-count rates are heavily state dependent, $\Gamma_0^{\mathrm{false}} \gg \Gamma_1^{\mathrm{false}}$. Nonetheless, we find that Eq. (12) also holds for all times t if the electron-tunneling rates fulfill $\Gamma_{\mathrm{in}} \approx \Gamma_{\mathrm{out}}$, see Sec. III B of the Supplemental Material [45].

With δS^{sys} given in Eq. (12), the systematic error of both the ordinary $\delta\kappa_m^{\mathrm{sys}} = \partial_\chi^m\delta S^{\mathrm{sys}}(e^\chi)|_{\chi=0}$ and factorial cumulants $\delta C_{F,m}^{\mathrm{sys}} = \partial_z^m\delta S^{\mathrm{sys}}(z)|_{z=1}$ can be determined. While the error of ordinary cumulants persists for all orders m, it is identically zero for factorial cumulants, $\delta C_{F,m}^{\mathrm{sys}} = 0$ for all orders $m > 1$. Since it is highly unlikely that the mean rates of false and missing counts are known exactly, the systematic error of ordinary cumulants $\delta\kappa_m^{\mathrm{sys}}$ cannot be corrected. Therefore, in this Letter, we suggest that factorial cumulants $C_{F,m}$ should always be used instead of ordinary cumulants κ_m when analyzing telegraph signals. Not only do they provide a superior way to characterize the measured probability distribution [35], but strikingly, they automatically cancel out systematic errors δS^{sys}, so that detailed knowledge of the specific value of the error is not required anymore. Thereby, factorial cumulants push the limits set by typical detection errors.

In summary, we demonstrated how quantum dynamics detected in real time can be evaluated by statistical means that are insensitive to typical, unavoidable experimental errors. The evaluation scheme is based on factorial cumulants, which are not influenced by any spurious signals caused by uncorrelated Poisson processes. Nevertheless, factorial cumulants contain the same information about the studied quantum system as ordinary cumulants [23,34–37]. Our Letter opens up a new perspective to gain precision in the analysis of existing and future experimental data [2–20]. For charge fluctuations in a self-assembled quantum dot, we demonstrated error reduction by orders of magnitude. We emphasize that our approach is purely passive, i.e., it leaves the studied quantum dynamics unchanged and thus allows for a high-precision analysis, so that, e.g., hidden quantum states, internal quantum transitions, and particle interactions can be revealed.

*eric.kleinherbers@uni-due.de

†psteg@mit.edu

[1] H.-P. Breuer and F. Petruccione, *The Theory of Open Quantum Systems* (Oxford University Press, Oxford, 2002).

[2] D. B. Hume, C. W. Chou, D. R. Leibrandt, M. J. Thorpe, D. J. Wineland, and T. Rosenband, Trapped-Ion State Detection Through Coherent Motion, Phys. Rev. Lett. **107**, 243902 (2011).

[3] F. D. Natterer, K. Yang, W. Paul, P. Willke, T. Choi, T. Greber, A. J. Heinrich, and C. P. Lutz, Reading and writing single-atom magnets, Nature (London) **543**, 226 (2017).

[4] S. Saskin, J. T. Wilson, B. Grinkemeyer, and J. D. Thompson, Narrow-Line Cooling and Imaging of Ytterbium Atoms in an Optical Tweezer Array, Phys. Rev. Lett. **122**, 143002 (2019).

[5] R. Zhou, S. Kunzelmann, M. R. Webb, and T. Ha, Detecting intramolecular conformational dynamics of single molecules in short distance range with subnanometer sensitivity, Nano Lett. **11**, 5482 (2011).

[6] Y. Choi, I. S. Moody, P. C. Sims, S. R. Hunt, B. L. Corso, I. Perez, G. A. Weiss, and P. G. Collins, Single-molecule lysozyme dynamics monitored by an electronic circuit, Science **335**, 319 (2012).

[7] H. S. Chung, K. McHale, J. M. Louis, and W. A. Eaton, Single-molecule fluorescence experiments determine protein folding transition path times, Science **335**, 981 (2012).

[8] N. Xin, J. Guan, C. Zhou, X. Chen, C. Gu, Y. Li, M. A. Ratner, A. Nitzan, J. F. Stoddart, and X. Guo, Concepts in the design and engineering of single-molecule electronic devices, Nat. Rev. Phys. **1**, 211 (2019).

[9] T. Miyamachi, M. Gruber, V. Davesne, M. Bowen, S. Boukari, L. Joly, F. Scheurer, G. Rogez, T. K. Yamada, P. Ohresser, E. Beaurepaire, and W. Wulfhekel, Robust spin crossover and memristance across a single molecule, Nat. Commun. **3**, 938 (2012).

[10] E. Burzurí, A. García-Fuente, V. García-Suárez, K. Senthil Kumar, M. Ruben, J. Ferrer, and H. S. J. van der Zant, Spin-state dependent conductance switching in single molecule-graphene junctions, Nanoscale **10**, 7905 (2018).

[11] F. Muckel, S. von Malottki, C. Holl, B. Pestka, M. Pratzer, P. F. Bessarab, S. Heinze, and M. Morgenstern, Experimental identification of two distinct skyrmion collapse mechanisms, Nat. Phys. **17**, 395 (2021).

[12] C. Guerlin, J. Bernu, S. Deléglise, C. Sayrin, S. Gleyzes, S. Kuhr, M. Brune, J.-M. Raimond, and S. Haroche, Progressive field-state collapse and quantum non-demolition photon counting, Nature (London) **448**, 889 (2007).

[13] S. N. Gupta, O. Bitton, T. Neuman, R. Esteban, L. Chuntonov, J. Aizpurua, and G. Haran, Complex plasmon-exciton dynamics revealed through quantum dot light emission in a nanocavity, Nat. Commun. **12**, 1310 (2021).

[14] J. P. Pekola, O.-P. Saira, V. F. Maisi, A. Kemppinen, M. Möttönen, Y. A. Pashkin, and D. V. Averin, Single-electron current sources: Toward a refined definition of the ampere, Rev. Mod. Phys. **85**, 1421 (2013).

[15] A. L. Efros and M. Rosen, Random Telegraph Signal in the Photoluminescence Intensity of a Single Quantum Dot, Phys. Rev. Lett. **78**, 1110 (1997).

[16] S. Gustavsson, R. Leturcq, B. Simovič, R. Schleser, T. Ihn, P. Studerus, K. Ensslin, D. C. Driscoll, and A. C. Gossard, Counting Statistics of Single Electron Transport in a Quantum Dot, Phys. Rev. Lett. **96**, 076605 (2006).

[17] C. Flindt, C. Fricke, F. Hohls, T. Novotný, K. Netočný, T. Brandes, and R. J. Haug, Universal oscillations in counting statistics, Proc. Natl. Acad. Sci. U.S.A. **106**, 10116 (2009).

[18] Y. Komijani, T. Choi, F. Nichele, K. Ensslin, T. Ihn, D. Reuter, and A. D. Wieck, Counting statistics of hole transfer in a *p*-type GaAs quantum dot with dense excitation spectrum, Phys. Rev. B **88**, 035417 (2013).

[19] S. Matsuo, K. Kuroyama, S. Yabunaka, S. R. Valentin, A. Ludwig, A. D. Wieck, and S. Tarucha, Full counting statistics of spin-flip and spin-conserving charge transitions in Pauli-spin blockade, Phys. Rev. Research **2**, 033120 (2020).

[20] H. Ott, Single atom detection in ultracold quantum gases: A review of current progress, Rep. Prog. Phys. **79**, 054401 (2016).

[21] B. Karimi, F. Brange, P. Samuelsson, and J. P. Pekola, Reaching the ultimate energy resolution of a quantum detector, Nat. Commun. **11**, 367 (2020).

[22] B. Karimi and J. P. Pekola, Quantum Trajectory Analysis of Single Microwave Photon Detection by Nanocalorimetry, Phys. Rev. Lett. **124**, 170601 (2020).

[23] E. Kleinherbers, P. Stegmann, and J. König, Revealing attractive electron–electron interaction in a quantum dot by full counting statistics, New J. Phys. **20**, 073023 (2018).

[24] A. Kurzmann, P. Stegmann, J. Kerski, R. Schott, A. Ludwig, A. D. Wieck, J. König, A. Lorke, and M. Geller, Optical Detection of Single-Electron Tunneling into a Semiconductor Quantum Dot, Phys. Rev. Lett. **122**, 247403 (2019).

[25] J. P. Garrahan and I. Lesanovsky, Thermodynamics of Quantum Jump Trajectories, Phys. Rev. Lett. **104**, 160601 (2010).

[26] F. Brange, A. Deger, and C. Flindt, Non-equilibrium phase transition in a single-electron micromaser, arXiv:2201.06131.

[27] J. H. Prechtel, A. V. Kuhlmann, J. Houel, L. Greuter, A. Ludwig, D. Reuter, A. D. Wieck, and R. J. Warburton, Frequency-Stabilized Source of Single Photons from a Solid-State Qubit, Phys. Rev. X **3**, 041006 (2013).

[28] J. Hansom, C. H. H. Schulte, C. Matthiesen, M. J. Stanley, and M. Atatüre, Frequency stabilization of the zero-phonon line of a quantum dot via phonon-assisted active feedback, Appl. Phys. Lett. **105**, 172107 (2014).

[29] T. Wagner, P. Strasberg, J. C. Bayer, E. P. Rugeramigabo, T. Brandes, and R. J. Haug, Strong suppression of shot noise in a feedback-controlled single-electron transistor, Nat. Nanotechnol. **12**, 218 (2017).

[30] A. Al-Ashouri, A. Kurzmann, B. Merkel, A. Ludwig, A. D. Wieck, A. Lorke, and M. Geller, Photon noise suppression by a built-in feedback loop, Nano Lett. **19**, 135 (2019).

[31] T. Wagner, P. Talkner, J. C. Bayer, E. P. Rugeramigabo, P. Hänggi, and R. J. Haug, Quantum stochastic resonance in an a.c.-driven single-electron quantum dot, Nat. Phys. **15**, 330 (2019).

[32] N. L. Johnson, A. W. Kemp, and S. Kotz, *Univariate Discrete Distributions* (Wiley, Hoboken, NJ, 2005).

[33] J. König and A. Hucht, Newton series expansion of bosonic operator functions, SciPost Phys. **10**, 7 (2021).

[34] C. W. J. Beenakker and H. Schomerus, Counting Statistics of Photons Produced by Electronic Shot Noise, Phys. Rev. Lett. **86**, 700 (2001).

[35] D. Kambly, C. Flindt, and M. Büttiker, Factorial cumulants reveal interactions in counting statistics, Phys. Rev. B **83**, 075432 (2011).

[36] P. Stegmann, B. Sothmann, A. Hucht, and J. König, Detection of interactions via generalized factorial cumulants in systems in and out of equilibrium, Phys. Rev. B **92**, 155413 (2015).

[37] P. Stegmann and J. König, Short-time counting statistics of charge transfer in Coulomb-blockade systems, Phys. Rev. B **94**, 125433 (2016).

[38] A. N. Vamivakas, C. Y. Lu, C. Matthiesen, Y. Zhao, S. Fält, A. Badolato, and M. Atatüre, Observation of spin-dependent quantum jumps via quantum dot resonance fluorescence, Nature (London) **467**, 297 (2010).

[39] A. Kurzmann, B. Merkel, P. A. Labud, A. Ludwig, A. D. Wieck, A. Lorke, and M. Geller, Optical Blocking of Electron Tunneling into a Single Self-Assembled Quantum Dot, Phys. Rev. Lett. **117**, 017401 (2016).

[40] P. Lochner, A. Kurzmann, J. Kerski, P. Stegmann, J. König, A. D. Wieck, A. Ludwig, A. Lorke, and M. Geller, Real-time detection of single Auger recombination events in a self-assembled quantum dot, Nano Lett. **20**, 1631 (2020).

[41] Y. Blanter and M. Büttiker, Shot noise in mesoscopic conductors, Phys. Rep. **336**, 1 (2000).

[42] S. Gustavsson, R. Leturcq, M. Studer, I. Shorubalko, T. Ihn, K. Ensslin, D. Driscoll, and A. Gossard, Electron counting in quantum dots, Surf. Sci. Rep. **64**, 191 (2009).

[43] M. B. Plenio and P. L. Knight, The quantum-jump approach to dissipative dynamics in quantum optics, Rev. Mod. Phys. **70**, 101 (1998).

[44] C. Flindt, T. Novotný, and A.-P. Jauho, Full counting statistics of nano-electromechanical systems, Europhys. Lett. **69**, 475 (2005).

[45] See Supplemental Material at http://link.aps.org/supplemental/10.1103/PhysRevLett.128.087701 for details on (I) the derivation of the error model, (II) the optical readout, and (III) the error resilience of factorial cumulants, which includes Refs. [46–48].

[46] G. C. Wick, A. S. Wightman, and E. P. Wigner, The intrinsic parity of elementary particles, Phys. Rev. **88**, 101 (1952).

[47] A. V. Khaetskii and Y. V. Nazarov, Spin-flip transitions between Zeeman sublevels in semiconductor quantum dots, Phys. Rev. B **64**, 125316 (2001).

[48] T. Brandes, Waiting times and noise in single particle transport, Ann. Phys. (Amsterdam) **17**, 477 (2008).